Estimating ice and unfrozen water in permafrost samples using industrial computed tomography scanning

Mahya Roustaei, Joel Pumple, Jordan Harvey, & Duane Froese
Department of Earth and Atmospheric Sciences – University of Alberta, Edmonton, Alberta, Canada

GeoCalgary 2022 October 2-5
Reflection on Resources

ABSTRACT
The relations between unfrozen water content and temperature in permafrost soils are important in cold regions engineering because much of the geomechanical behavior of permafrost depends on ice content which can vary with temperature. X-ray computed tomography (CT) scanning is a method with applications in geoscience, soil science, and geotechnical engineering that has shown potential in permafrost research. In this study, we use an industrial CT scanner, as opposed to the more common medical CT scanners that have been previously used, to establish relations between the ice, sediment, and unfrozen water content of a clayey soil at -1, -3, -6, and -12 °C. High-resolution CT scans were compared with time-domain reflectometry (TDR) records of unfrozen water content. Image processing results showed 12.8% increase in the ice volume of the sample at colder temperatures accompanying a 14.5 % decrease in water content tracked by TDR. The expansion of ice lenses at colder temperatures was also visualized in CT images. The extracted changes from image processing and TDR records were more significant between lower temperatures due to more unfrozen water contents.

RÉSUMÉ
Les relations entre la teneur en eau non gelée et la température dans les sols de pergélisol sont importantes dans l'ingénierie des régions froides car une grande partie du comportement géomécanique du pergélisol dépend de la teneur en glace qui peut varier avec la température. La tomodensitométrie (TDM) à rayons X est une méthode avec des applications en géoscience, en science du sol et en génie géotechnique qui a montré un potentiel dans la recherche sur le pergélisol. Dans cette étude, nous utilisons un tomodensitomètre industriel, par opposition aux tomodensitomètres médicaux plus courants qui ont été utilisés auparavant, pour établir des relations entre la teneur en glace, en sédiments et en eau non gelée d'un sol argileux à -1, -3, -6 et -12 °C. Des tomodensitogrammes à haute résolution ont été comparés aux enregistrements de réflectométrie dans le domaine temporel (TDR) de la teneur en eau non gelée. Les résultats du traitement d'image ont montré une augmentation de 12,8 % du volume de glace de l'échantillon à des températures plus froides accompagnant une diminution de 14,5 % de la teneur en eau suivie par le TDR. L'expansion des lentilles de glace à des températures plus froides a également été visualisée dans les images CT. Les changements extraits du traitement d'image et des enregistrements TDR étaient plus significatifs entre des températures plus basses en raison d'une plus grande teneur en eau non gelée.

1 INTRODUCTION

Unfrozen water exists as a thin film of liquid water on mineral surfaces in fine-grained soils at below-freezing temperatures, and plays an important role in the determination of a soil's thermophysical response to changing physical and environmental conditions (Williams, 1964; Hoekstra, 1966; Anderson and Tice, 1971; Darrow et al., 2011). The amount and distribution of unfrozen water is dependent, primarily on soil temperature and salinity, and changes strongly as temperatures warm toward 0ºC, and unfrozen water can exist in clays at temperatures below -60ºC (Anderson and Tice, 1971). The distribution and freezing of water strongly impact frost heaving, mechanical properties and thermal regime of frozen ground (Williams, 1964; Hoekstra, 1966; Aksenov et al., 1998; Romanovsky & Osterkamp, 2000; Torrance et al., 2008; Darrow, 2011).

Measuring unfrozen water in frozen soils began with the pioneering dilatometer work by Bouyoucos (1917, 1920) and continued with additional methods such as differential scanning calorimetry (DSC), time-domain reflectometry (TDR), and the pulsed nuclear magnetic resonance (P-NMR) method (Anderson and Tice 1973, Kruse and Darrow 2017)

Williams (1964) reported freezing data for silty soil, and measurements of unfrozen water content with a calorimeter. In 2006, Flerchinger et al. used TDR and thermocouples in the field at depths of 5 and 10 cm during the fall-winter season in order to measure the unfrozen water content. In 2011, Watanabe et al. also used TDRs in a column freezing experiment in three different unsaturated soils to obtain a detailed dataset of temperature, water content, and pressure-head change under freezing conditions. They first calibrated the TDR measurements of unfrozen water content by comparison with the P-NMR measurement in their study, and showed that liquid water content decreased strongly in the sand, more gradually in the loam, and at variable speeds in the silt loam. Zhou et al. (2014) combined TDR and an Am-241 gamma ray source to measure unfrozen water content and ice content in frozen soil simultaneously. Their results indicate that these two methods have similar accuracy and response to changes in water content.

Kruse & Darrow (2017) measured unfrozen water content using a refined pulsed nuclear magnetic resonance

(P-NMR) testing facility and the normalization method, which yielded accurate and repeatable results. They showed that cation treatments have a negligible effect on the unfrozen water content of kaolinite, illite, and chlorite.

Over the last several decades there was a rapid advance in using non-destructive methods for the structural investigation of materials. One of these techniques is micro-computed tomography (μCT) which has been applied successfully to the fields of geoscience, soil science, and geotechnical engineering in order to quantify macro/micro characteristics including cryotextures, soil fabric, and fluid movement through soil cores (Peyton et al. 1992, Ketcham and Carlson 2001a, Blair et al. 2007, Taina et al. 2008, Luo et al. 2008, Helliwell et al. 2013, Darrow and Lieblappen 2020).

CT has been a useful tool in permafrost research since the initial studies (e.g. Calmels and Allard 2004). Recent work has focused on cryostructures (Calmels et al., 2012), excess ice determination (Lapalme et al. 2017), distribution and consolidation of soil between ice lenses (Torrance et al. 2008), soil degradation in freeze-thaw cycles (Nguyen et al., 2019; Wang et al., 2018, Wang 2017), and quantification of micro lenticular ice lens formation (Darrow and Lieblappen 2020). However, to our knowledge, there are few studies that test the application of CT in quantifying the unfrozen water content of frozen soils. The present study was conducted to test the capability of the CT method in establishing the ice, sediment, and unfrozen water contents of a clayey soil at -1, -3, -6, and -12 °C via Industrial CT scanning.

2 MATERIALS

2.1 Soil

In this study, an EPK Kaolin, manufactured by Edgar Minerals Inc. and classified as MH in the Unified Soil Classification System was used. The soil properties are presented in Table 1.

Table 1. Characteristics of tested soil (Palat et al. 2019)

Liquid Limit (%)	58
Plastic Limit (%)	41.5
Plasticity Index (%)	16.4
Optimum Moisture Content (OMC) (%)	28
Maximum Dry Density (kN/m^3)	15.2

3 EXPERIMENTAL PROCEDURE

3.1 Sample preparation and temperature control

The sediment was housed in a 50ml falcon tube (Figure 1a), saturated to a liquid limit of 58%, and homogenized to ensure the moisture was evenly distributed. A soil temperature sensor (Meter RT-1) and moisture sensors/TDR (Meter EC-5) were inserted into the center top half of the falcon tube. The sample was then carefully placed in a -20 C chest freezer ensuring that the probes stayed in the ideal center position while freezing. During the CT scans the sample was housed in a styrofoam container with additional foam surrounding the falcon tube to hold temperature steady (Figures 1b, and c). Depending on the target temperature, an ice pack was added to the top half of the container to help stabilize the tube's internal temperature over the 15-minute scan time.

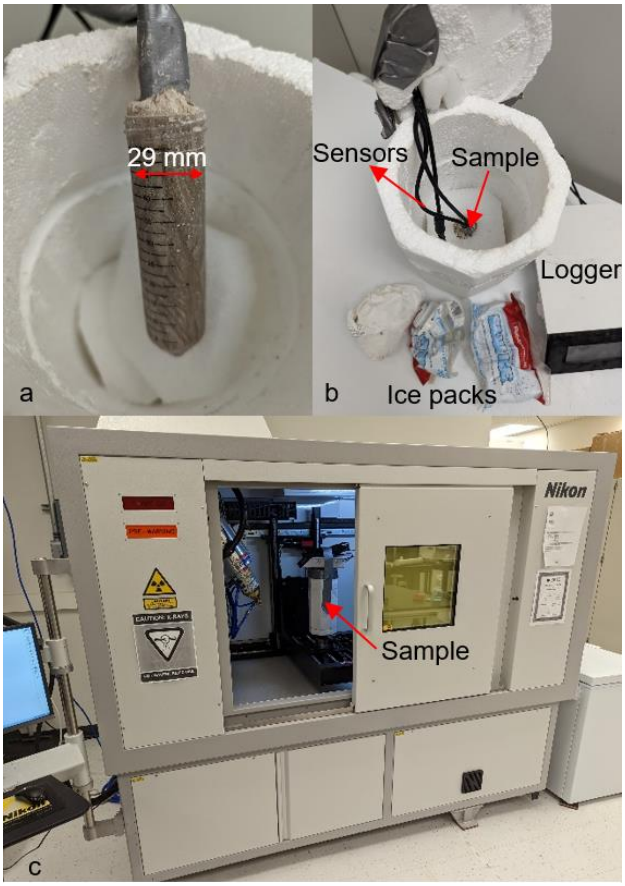

Figure 1. a) Frozen clayey sample in falcon tube with inserted sensors a) sample container b) sample location in CT machine

3.2 Sensors

The Sensors used were the Meter RT-1 soil temperature sensor and the EC-5 soil moisture sensor. The RT-1 has a temperature resolution of 0.1°C and an accuracy of +/-1°C for the temperatures discussed in this study. The EC-5 has a moisture content resolution of 0.001 m^3/m^3 and an accuracy of +/- 0.03 m^3/m^3. These sensors were connected to a Meter ZL6 data logger and data was collected every five minutes. The data logger was also connected to a smartphone via Bluetooth during the scans to allow for continuous monitoring of the internal temperature to confirm the scan was collected under stable conditions.

The probes were connected to the data logger while the sample was in the freezer to monitor internal temperature. Once the desired internal temperature was confirmed, the ice block was added to the container and the container was sealed and moved into the CT Scanner to begin the acquisition. We found that if the ice block accompanying the sample tube was held at -10°C prior to the -0.8°C, and -3.1°C scans, it would hold the tube temperature within 0.1°C of the start temperature over the duration of the scan. However, for the -6°C and -12°C scans, the ice block needed to be held at -20°C prior to the scan to best stabilize tube temperature. This simple sample housing and temperature control approach worked well with our CT scanner as it does not require an external chiller and is constructed with a material that is almost invisible in the x-ray images (Figure 2).

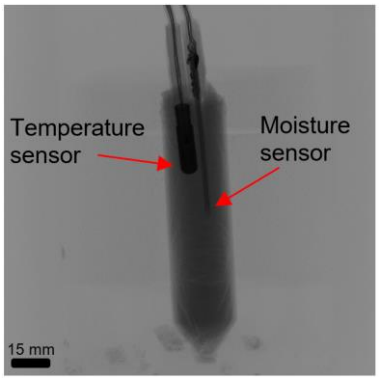

Figure 2. X-ray image of the sample

3.3 Scanning and image processing

Micro Computerized tomography (uCT) was used to examine the ice, sediment and unfrozen water content of the clayey soil samples at varying temperatures. This method is a non-destructive observational technique that has been useful in the investigation of geological porous media (Ketcham and Carlson 2001b, Kozaki et al. 2001, van Geet et al. 2005). It consists firstly in recording a set of two-dimensional X-ray radiographs at multiple angles (typically 180 or 360 degrees), and secondly reconstructing the 2D slices from the radiographs using a mathematical algorithm. The final 3D image of the internal structure is obtained by stacking the slices. The final measurement is the linear attenuation coefficient which depends on the density and the atomic number of the material (Ketcham & Carlson, 2001; Saba et al., 2014; van Geet et al., 2005). This varies slightly from most earlier permafrost CT studies that report values in Hounsfield units that are common from medical CT studies (eg. Calmels et al., 2010). In this study we use the primary linear attenuation values derived from the CT data.

The scans presented here were carried out with a Nikon XTH 225 ST and the soil samples were scanned at 140 Kv and rotated 360° with an exposure time of 67 ms, resulting in a voxel (3D volume element representing pixel resolution and slice thickness) of 25 µm. The images were reconstructed into three-dimensional gray-scale volumes using CT pro 3D software and finally analyzed using Dragonfly 2022 image processing software.

4 RESULTS

Figures 3a and b present CT slices of the frozen clayey sample. This slice is presenting the gray levels corresponding to X-ray attenuation, which reflects the proportion of X-rays scattered or absorbed by different materials of the sample as they pass through each voxel (volume elements). Clayey particles as the denser materials (1.5-2 g/cm^3) appear lighter while ice lenses and falcon tube that have almost the same density (0.8-0.9 g/cm^3) appear darker. Air with the lowest density is the black seen surrounding the tube.

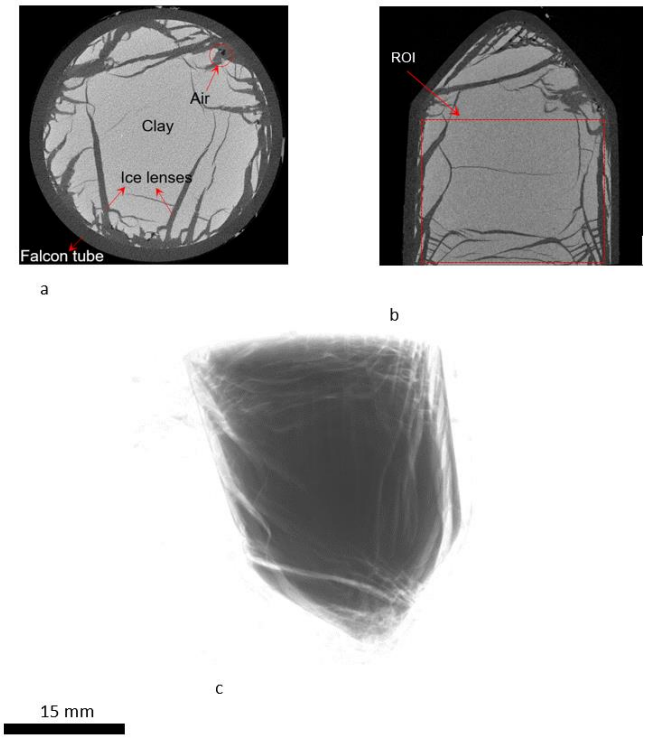

Figure 3. a) Horizontal section, b) vertical section, and 3D CT images of frozen clay

A typical reconstructed 3D image of the frozen clayey sample is presented in figure 3c. These figures are clearly showing that the effective pixel size of scans (25 µm) was appropriate enough to clearly show the ice lens formation that started from the edges, closest to the freezing front, and extended towards the center of the sample.

In CT, the ability to differentiate materials depends on their respective linear attenuation coefficients, the linear attenuation coefficient (µ) characterizes how easily a volume of material can be penetrated by a beam of X-rays. So materials with very divergent densities and/or atomic constituents are easy to differentiate (Kyle and Ketcham 2015). As a result, differentiating between ice and water with just 8.2% of density difference (considering 0.917 g/cm^3 for ice compared to 0.999 g/cm^3 for water) and in very small pores is a significant challenge.

In order to quantify the amount of ice or unfrozen water contents between scans and eliminate the effect of the falcon tube with a similar density to ice, the following image processing steps were adopted in this study. First, a cylinder with 25 mm diameter and 25 mm height was selected from the same location of each scan (figure 3b) as the region of interest (ROI) and the Otsu algorithm was applied to it. In image processing the Otsu algorithm, proposed by Nobuyuki Otsu in 1979, performs the automatic clustering-based image thresholding. In this method, it is presumed that there are two classes of pixels that are "*foreground*" pixels and "*background*" pixels of the image. The optimum thresholding is calculated by distinguishing the two classes so that the minimum class variance can be obtained (Kumar & Tiwari, 2019). This method was applied to the selected ROIs to differentiate sediments and ice/water. Figure 4 shows the foreground and background of two Otsu algorithms applied on selected ROI in the -0.7 ºC scan. The first foreground shows sediments or clayey particles as the densest material while the first background is ice lens formations that can also be separated into two parts by applying the second Otsu algorithm. Hence, the foreground part of the second algorithm is the portion of ice lenses with a higher density while the background corresponds to the ice/material with the lowest density within the whole ROI.

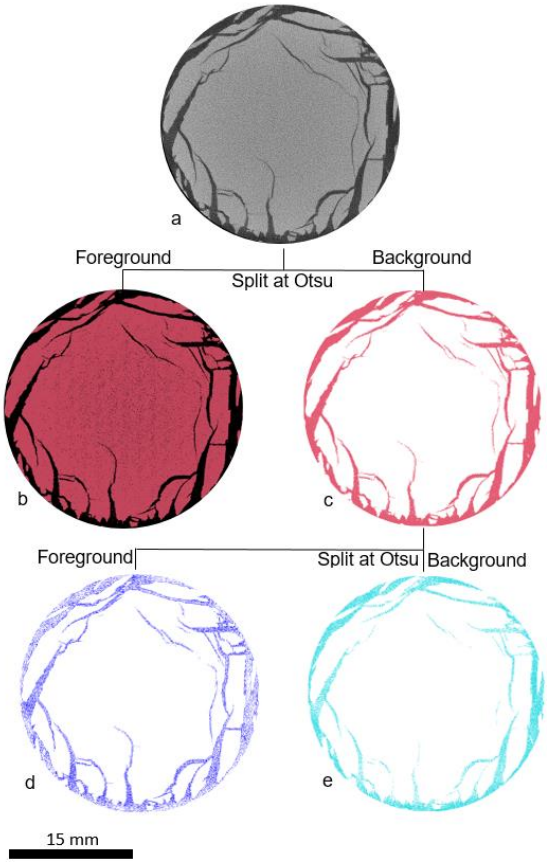

Figure 4. a) ROI of the frozen clay sample at -0.7 ºC, b) foreground of ROI (first Otsu algorithm), c) background of ROI (first Otsu algorithm), d) foreground of ROI (second Otsu algorithm), and e) background of ROI (second Otsu algorithm)

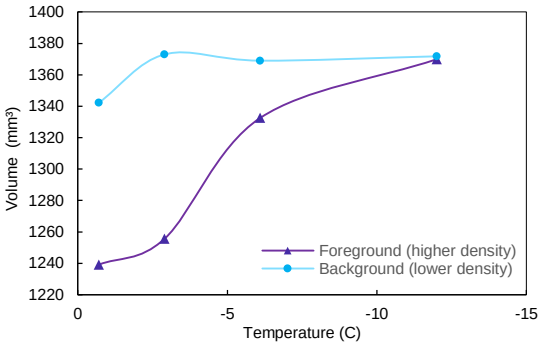

Figure 5. Volume variations of two ice intervals vs temperature

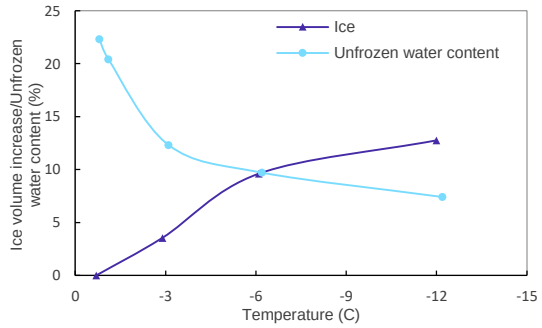

Figure 6. TDR recordings and ice volumes vs temperature

Image processing of scans shows that the resulting intervals from the Otsu thresholding method vary with temperature. Figure 5 shows the volume variation of ice intervals in different scans and indicates that the volume of ice increases at colder temperatures (more significant from -0.7 to -6 ºC). This could represent a transferring of unfrozen water content to ice. In addition, the volume increase is more significant in the foreground interval with higher density (closer to the water) in comparison with the background one.

To compare these changes with TDR data, the total volume increase of the ice intervals was plotted with the TDR data in figure 6. The decreasing trend of water content at colder temperatures corresponds with an increase in the ice volume of the sample. The total increase in the volume of the two ice intervals is 12.8% from -0.7 to -12 ºC while TDR recordings showed a 14.9 % decrease in the water content between these temperatures. The slight difference (15%) in these two amounts could reflect unfrozen water at the bottom cone part of the falcon tube that was not included in the cylinder ROI.

For better visualization of ice expansion at colder temperatures, changes of a specific small ice lens during scans were shown in density color masked slices in figure 7 at a) -0.7, b) -2.9, c) -6.1, and d) -12 ºC. This figure shows an expansion of ice lenses as well as the generation of new lenses at colder temperatures as unfrozen water transforms to ice. Similar to figure 5, the main changes occur at lower temperatures (-0.7 to -6.1ºC) with higher unfrozen water contents.

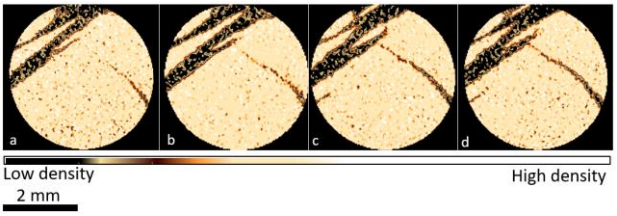

Figure 7. Visualization of changes in ice lenses in a) -0.7, b) -2.9, c) -6.1, and d) -12 ºC

5 CONCLUSION

The relationship between unfrozen water content and temperature in a Kaolin clayey frozen soil was investigated in this study. For this purpose, an industrial CT scanner was used to establish relations between the ice, sediment, and unfrozen water content of the soil at -1, -3, -6, and -12 °C and were compared with TDR data.

Based on these results the following main conclusions can be drawn:

- Image processing results showed 12.8% increase in the ice volume of the sample at colder temperatures accompanying a 14.5 % decrease in water content tracked by TDR.
- The significant portion of volume increase occurred in the ice interval with the higher density that could reflect the transformation of unfrozen water to ice.
- CT images show the expansion of existing ice lenses as well as the generation of new ones at colder temperatures reflecting unfrozen water migration and transformation to ice.

Collectively, the results of this study show a promising approach for establishing temperature-dependent physical properties for a clayey sample. This approach shows promise for future development using a variety of natural and synthetic permafrost samples in the future.

6 References

Aksenov, V.I., Klinova, G.I., and Scheikin, I. v. 1998. Material composition and strength characteristics of saline frozen soils. *In* The 7Th Intl.Permafrost Conf. pp. 1–4.

Anderson, D.M., and Tice, A.R. 1973. The unfrozen interfacial phase in frozen soil water systems. In: Ecological Studies: Analysis and Synthesis.

Blair, J.M., Falconer, R.E., Milne, A.C., Young, I.M., and Crawford, J.W. 2007. ModelingThree-Dimensional Microstructure in Heterogeneous Media. Soil Science Society of America Journal, **71**(6): 1807–1812. doi:10.2136/sssaj2006.0113.

Bouyoucos, G. 1920. A new classification of the soil moisture. Soil Science, **11**(1): 33–47.

Bouyoucos, G.W. 1917. Classification and Measurement of the Different Forms of Water in the Soil by Means of the Dilatometer Method.

Calmels, F., and Allard, M. 2004. Ice segregation and gas distribution in permafrost using tomodensitometric analysis. Permafrost and Periglacial Processes, **15**(4): 367–378. doi:10.1002/ppp.508.

Darrow, M.M. 2011. Thermal modeling of roadway embankments over permafrost. Cold Regions Science and Technology, **65**(3): 474–487. doi:10.1016/j.coldregions.2010.11.001.

Darrow, M.M., and Lieblappen, R.M. 2020. Visualizing cation treatment effects on frozen clay soils through µCT scanning. Cold Regions Science and Technology, **175**. Elsevier B.V. doi:10.1016/j.coldregions.2020.103085.

Flerchinger, G.N., Seyfried, M.S., and Hardegree, S.P. 2006. Using Soil Freezing Characteristics to Model Multi-Season Soil Water Dynamics. Vadose Zone Journal, **5**(4): 1143–1153. doi:10.2136/vzj2006.0025.

van Geet, M., Volckaert, G., and Roels, S. 2005. The use of microfocus X-ray computed tomography in characterising the hydration of a clay pellet/powder mixture. Applied Clay Science, **29**(2): 73–87. doi:10.1016/j.clay.2004.12.007.

Helliwell, J.R., Sturrock, C.J., Grayling, K.M., Tracy, S.R., Flavel, R.J., Young, I.M., Whalley, W.R., and Mooney, S.J. 2013. Applications of X-ray computed tomography for examining biophysical interactions and structural development in soil systems: a review. European Journal of Soil Science, **64**(3): 279–297. doi:10.1111/ejss.12028.

Hoekstra, P. 1966. Moisture movement in soils under temperature gradients with the cold-side temperature below freezing. Water Resources Research, **2**(2): 241–250. doi:10.1029/WR002i002p00241.

Ketcham, R.A., and Carlson, W.D. 2001a. Acquisition, optimization and interpretation of X-ray computed tomographic imagery: applications to the geosciences. Computers & Geosciences, **27**(4): 381–400. doi:10.1016/S0098-3004(00)00116-3.

Ketcham, R.A., and Carlson, W.D. 2001b. Acquisition, optimization and interpretation of X-ray computed tomographic imagery: applications to the geosciences. Computers & Geosciences, **27**(4): 381–400. doi:10.1016/S0098-3004(00)00116-3.

Kozaki, T., Suzuki, S., Kozai, N., Sato, S., and Ohashi, H. 2001. Observation of Microstructures of Compacted Bentonite by Microfocus X-Ray Computerized Tomography (Micro-CT). Journal of Nuclear Science and Technology, **38**(8): 697–699. doi:10.1080/18811248.2001.9715085.

Kruse, A.M., and Darrow, M.M. 2017. Adsorbed cation effects on unfrozen water in fine-grained frozen soil measured using pulsed nuclear magnetic resonance. Cold Regions Science and Technology, **142**: 42–54. Elsevier B.V. doi:10.1016/j.coldregions.2017.07.006.

Kumar, and Tiwari. 2019. A Comparative Study of Otsu Thresholding and K-means Algorithm of Image Segmentation. International Journal of Engineering and Technical Research (IJETR) , **9**(5).

Kyle, J.R., and Ketcham, R.A. 2015. Application of high resolution X-ray computed tomography to mineral deposit origin, evaluation, and processing. Ore

Geology Reviews, **65**(P4): 821–839. Elsevier. doi:10.1016/j.oregeorev.2014.09.034.

Lapalme, C.M., Lacelle, D., Pollard, W., Fortier, D., Davila, A., and McKay, C.P. 2017. Cryostratigraphy and the Sublimation Unconformity in Permafrost from an Ultraxerous Environment, University Valley, McMurdo Dry Valleys of Antarctica. Permafrost and Periglacial Processes, **28**(4): 649–662. doi:10.1002/ppp.1948.

Luo, L., Lin, H., and Halleck, P. 2008. Quantifying Soil Structure and Preferential Flow in Intact Soil Using X-ray Computed Tomography. Soil Science Society of America Journal, **72**(4): 1058–1069. doi:10.2136/sssaj2007.0179.

Nguyen, T.T.H., Cui, Y.-J., Ferber, V., Herrier, G., Ozturk, T., Plier, F., Puiatti, D., Salager, S., and Tang, A.M. 2019. Effect of freeze-thaw cycles on mechanical strength of lime-treated fine-grained soils. Transportation Geotechnics, **21**: 100281. doi:10.1016/j.trgeo.2019.100281.

Otsu, N. 1979. A Threshold Selection Method from Gray-Level Histograms. IEEE Transactions on Systems, Man, and Cybernetics, **9**(1): 62–66. doi:10.1109/TSMC.1979.4310076.

Palat, A., Roustaei, M., and Hendry, M. 2019. Effect of fiber content on the mechanical behavior of fiber-reinforced clay. *In* GeoSt.John's 2019. St.John's.

Peyton, R.L., Haeffner, B.A., Anderson, S.H., and Gantzer, C.J. 1992. Applying X-ray CT to measure macropore diameters in undisturbed soil cores. Geoderma, **53**(3–4): 329–340. doi:10.1016/0016-7061(92)90062-C.

Romanovsky, V.E., and Osterkamp, T.E. 2000. Effects of unfrozen water on heat and mass transport processes in the active layer and permafrost. Permafrost and Periglacial Processes, **11**(3): 219–239. doi:10.1002/1099-1530(200007/09)11:3<219::AID-PPP352>3.0.CO;2-7.

Saba, S., Barnichon, J.-D., Cui, Y.-J., Tang, A.M., and Delage, P. 2014. Microstructure and anisotropic swelling behaviour of compacted bentonite/sand mixture. Journal of Rock Mechanics and Geotechnical Engineering, **6**(2): 126–132. doi:10.1016/j.jrmge.2014.01.006.

Taina, I.A., Heck, R.J., and Elliot, T.R. 2008. Application of X-ray computed tomography to soil science: A literature review. Canadian Journal of Soil Science, **88**(1): 1–19. doi:10.4141/CJSS06027.

Torrance, J.K., Elliot, T., Martin, R., and Heck, R.J. 2008. X-ray computed tomography of frozen soil. Cold Regions Science and Technology, **53**(1): 75–82. doi:10.1016/j.coldregions.2007.04.010.

Wang, S., Yang, P., and Yang, Z. (Joey). 2018. Characterization of freeze–thaw effects within clay by 3D X-ray Computed Tomography. Cold Regions Science and Technology, **148**: 13–21. doi:10.1016/j.coldregions.2018.01.001.

Watanabe, K., Kito, T., Wake, T., and Sakai, M. 2011. Freezing experiments on unsaturated sand, loam and silt loam. Annals of Glaciology, **52**(58): 37–43. doi:10.3189/172756411797252220.

Williams, P.J. 1964. Unfrozen Water Content of Frozen Soils and Soil Moisture Suction. Géotechnique, **14**(3): 231–246. doi:10.1680/geot.1964.14.3.231.

Zhou, X., Zhou, J., Kinzelbach, W., and Stauffer, F. 2014. Simultaneous measurement of unfrozen water content and ice content in frozen soil using gamma ray attenuation and TDR. Water Resources Research, **50**(12): 9630–9655. doi:10.1002/2014WR015640.